Investigation of the Reaction between Fe_2O_3 and Al Accomplished by Ball Milling and Self-Propagating High-Temperature Techniques

Giacomo Cao[a], Giorgio Concas[b], Anna Corrias[c], Roberto Orru'[a], Giorgio Paschina[c], Barbara Simoncini[a], and Giorgio Spano[b]

[a] Dipartimento di Ingegneria Chimica e Materiali, Universita' degli Studi di Cagliari, Piazza d'Armi, I-09123 Cagliari, Italy
[b] Dipartimento di Scienze Fisiche, Universita' degli Studi di Cagliari e Istituto Nazionale di Fisica della Materia, Via Ospedale 72, I-09124 Cagliari, Italy
[c] Dipartimento di Scienze Chimiche, Universita' degli Studi di Cagliari, Via Ospedale 72, I-09124 Cagliari, Italy

Z. Naturforsch. **52a**, 539–549 (1997); received April 25, 1997

In this work we investigate the mechanism of product formation of the aluminothermic reaction of Fe_2O_3 in the presence of Al_2O_3 using Ball Milling and Self-propagating High-temperature techniques.

Results obtained by experiments under either argon or air atmosphere are analysed by X-ray diffraction and Mössbauer spectroscopy, together with microstructure observations. It is shown that ball milling products are strongly affected by the kind of atmosphere, while self-propagating high-temperature ones are only weakly influenced. Reaction mechanisms taking place in these cases are proposed.

While ball milling involves only solid state reactions, the formation of a melt occurs under self-propagating high-temperature conditions.

Key words: Aluminothermic reduction, Ball Milling, Self-propagating High-temperature Synthesis, Mössbauer spectroscopy, X-ray diffraction, Mechanism of reaction.

1. Introduction

The reaction between hematite (Fe_2O_3) and aluminum belongs to a broad class of highly exothermic reactions, namely thermite reactions, where a metallic or non-metallic oxide is reduced by a metal to form a more stable oxide and the corresponding metal or non-metal of the reactant oxide [1]. Thermite reactions have attracted the attention of researchers and technologists due to their industrial applications such as the synthesis of refractory ceramic and composite materials [2], welding and the preparation of ceramic linings in metallic pipes [3–6].

Despite of the various applications of thermite reactions, few mechanistic investigations of the chemical transformations involved are available in the literature [1]. In particular, for the case of the aluminothermic reduction of ferric oxide, Korchagin and Podergin [7] studied the interaction of hematite particles on aluminum film using high-temperature diffraction electron microscopy. More recently, Orru' et al. [8, 9] examined the mechanism of structure and product formation of the aluminothermic reduction of hematite under Self-propagating High-temperature Synthesis (SHS) conditions in the presence of alumina as diluent by taking advantage of the so-called Combustion Front Quenching (CFQ) technique.

SHS represents a relatively new technique for the preparation of advanced materials. It is based on the concept that by igniting the starting mixture by means of an external energy source for relatively short times, a highly exothermic reaction may propagate in the form of a self-sustained combustion wave leading to reaction products progressively, without requiring additional energy. This technique represents an attractive alternative to conventional methods of material synthesis due to the simplicity of the process and its relatively low energy requirements, the higher purity of products, and the possibility of obtaining complex or metastable phases [10–13].

Ideally, the mechanism of SHS reactions should be studied by following *in situ* the propagation of the combustion front. This goal could be accomplished by using the synchrotron radiation technique [14] which makes it possible to trace reactions taking place during high temperature combustion synthesis. However,

Reprint requests to Prof. G. Cao; Fax 39 70 675 5067.

0932-0784 / 97 / 0600-0539 $ 06.00 © – Verlag der Zeitschrift für Naturforschung, D-72027 Tübingen

this method of investigation involves various difficulties in the experiments and in their interpretation [15]. A simpler approach is provided for example by the CFQ technique, which is based on the rapid quenching of the reaction front during its propagation. This method is able to simultaneously freeze the intermediate and end reaction products so that the evolution of the combustion synthesis can be followed by characterizing the region of the sample where the reaction wave is arrested. Combustion front quenching could be obtained for example by dropping the reacting sample in liquid argon or by using a massive copper wedge to induce higher heat losses [15].

Also Ball Milling (BM) techniques have shown to be suitable to prepare similar systems by the activation of solid state reactions. Repeated fracture and cold welding of powder particles can give rise to an intimate mixing at atomic level which promotes interdiffusion of the starting components, an essential condition for the reaction to take place.

BM has been largely applied to obtain amorphous and nanocrystalline alloys starting from elemental components [16, 17]. More recently, it has been applied to the preparation of composite materials through displacement reactions such as

$$M_xO_y + zR \rightarrow xM + R_zO_y,$$

where M is a metal and R can be either Al [18–20] or Si [18, 20–22].

The BM offers a way to control the evolution of the reaction so that its path can be studied; in fact, the energy involved in the ball milling can be fixed by properly choosing the process parameters (i.e. milling mechanics, diameter of balls, ball/powder weight ratio).

With the aim of better elucidating the reaction path of the aluminothermic reduction of hematite, we compare in this work the results obtained under SHS conditions, either with or without front quenching, with those resulting from the use of BM technique. This goal is accomplished by characterizing in details intermediate phases and final products by means of an extensive use of X-ray diffraction and Mössbauer spectroscopy, together with microstructure observations. The aim is also to demonstrate that BM may be considered as a valuable complementary tool to identify reaction mechanisms involved in SHS processes.

It is worth noting that, since for technological applications diluents need to be added to the starting mixture in order to reduce the violent character of thermite reactions, alumina is used for this purpose in the present work.

2. Experimental Procedure

Hematite (Aldrich Chemical Company Inc., purity $> 99\%$, av. particle size $< 5\ \mu m$) and aluminum (Aldrich Chemical Company Inc., purity 99%, av. particle size 200 mesh) in stoichiometric ratio according to the reaction $Fe_2O_3 + 2\,Al \rightarrow 2\,Fe + Al_2O_3$ and 25% wt of alumina (Aldrich Chemical Company Inc., purity 99.8%, av. particle size $< 10\ \mu m$) were used in powder form as received.

A centrifugal mill (Tecnotest, Italy), operating for about six hours, is employed to prepare the reacting mixture, using acetone as dispersing agent. Scanning electron microscopy (SEM) allowed us to verify that a good intermixture was achieved.

The reaction was carried out be means of two different techniques, i.e. BM and SHS, either under argon or air atmosphere.

BM experiments were performed in a Spex 8000 vibratory mill. 5 grams of the reacting mixture were sealed in a stainless stell vial with balls of the same material (4 balls 8 mm$\varnothing$ + 4 balls 10 mm$\varnothing$), using a full/void volume ratio and a ball/powder weight ratio of 1/20 and of 5/1, respectively. Sealing was performed either in a glove box filled with argon (< 10 ppm O_2, < 10 ppm H_2O) or under air. Overheating of the vial was prevented by alternating milling and rest periods at 5 minute intervals. About 0.2 g of the reacting mixture were sampled at different milling times either in a glove box filled with argon or under air atmosphere.

SHS and CFQ experiments were conducted using the set-up schematically shown in Figure 1. It consists of a reaction vessel, where the desired atmosphere can be obtained by means of suitable gas cylinder, a power supply (Belotti, Italy; output 0–100 V) which provides the energy required for reaction ignition, an infrared pyrometer (Land Instrument, Cyclops 152 A model), a video recorder (JVC, AG 4700 model), which allowed us to record the reaction evolution, and a computer system (Power Macintosh 7200), which not only drives the power supply to produce a well-defined energy pulse but also is equipped with a data acquisition board (Model PCI-MIO-16 XE-50, National Instruments) supported by a software package (LabVIEW, National Instruments).

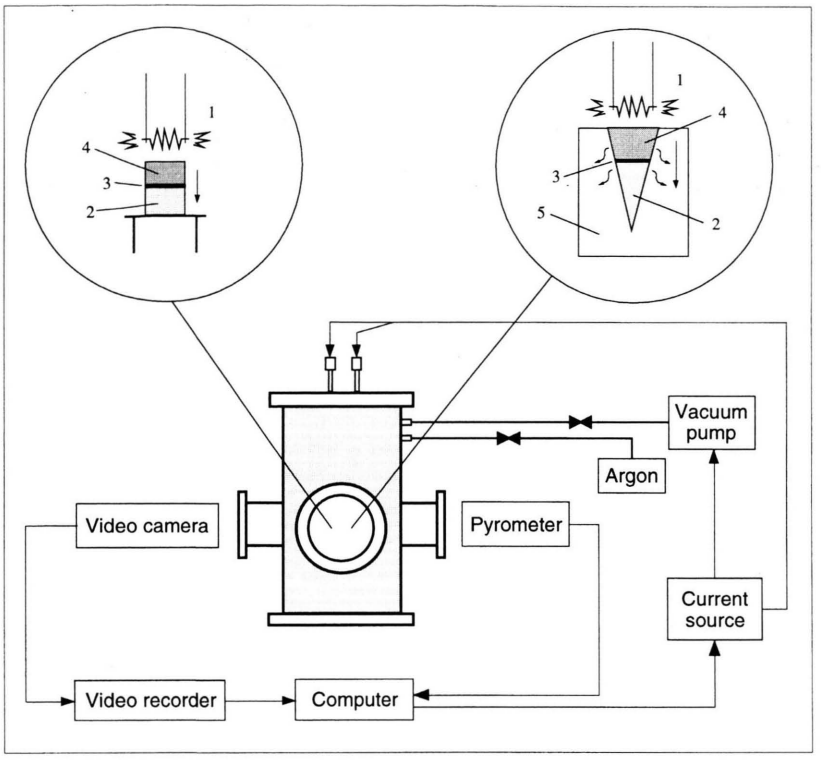

Fig. 1. Schematic representation of the experimental set-up to obtain SHS and CFQ samples:
1) tungsten coil,
2) starting mixture,
3) reaction front,
4) final products,
5) bulk copper block.

SHS experiments were conducted using cylindrical pellets (15 mm in diameter and 20 mm high) obtained by pressing about 8 grams of the reacting mixture, once dried in air in order to totally eliminate acetone, in a uniaxial single-acting press (RMU, Italy) at approximately 10 kN for one minute.

The cylindrical copper block (105 mm high with a base diameter of 65 mm) with a wedge shaped notch (50 mm high with a base diameter of 20 mm) depicted in Fig. 1, was employed to perform CFQ experiments. A total mass of about 14 grams of the starting mixture was pressed inside the copper block, under the same conditions used for preparing cylindrical pellets.

The green densities of the pellets with cylindrical and conical shape were determined from mass and geometric measurements and were equal to 2.3 and 2.67 g/cm^3, which represent approximately the 51% and 60% of the theoretical value, respectively.

In a typical SHS experiment, the cylindrical pellet was placed into the vessel and the reaction was initiated at its base by means of a tungsten coil (R. D. Mathis Company, USA) connected to the power supply depicted in Fig. 1, which was programmed to produce an energy pulse by setting 20 volts for about 4 seconds. This interval was selected so that the energy source is turned off as soon as the reaction is initiated. The same ignition procedure was followed when considering the CFQ samples. However, in this case the combustion reaction propagates towards the wedge's apex and is extinguished due to the combination of intense heat removal by the copper block and the shrinkage of the cross section. Simultaneously, intermediate and final products are quenched and the evolution of the structure, during preheating, combustion and post-combustion, can be followed by studying product microstructure and composition at different areas relatively to the location where the combustion front was extinguished.

The reproducibility of the experimental runs was verified by repeating each of them at least twice, regardless of the technique employed, i.e. BM, SHS, and CFQ.

A summary of the samples obtained by means of the techniques described above is reported in Table 1.

X-ray diffraction (XRD) spectra were recorded using CuKα radiation on a $\theta-\theta$ Seifert X3000 diffrac-

Table 1. Samples obtained by BM, SHS and CFQ techniques, under argon or air atmosphere.

Sample identification	Technique	Atmosphere	Sample type
BMAr	BM	Argon	Powder
BMA	BM	Air	Powder
SHSAr	SHS	Argon	Cylindrical pellet
SHSA	SHS	Air	Cylindrical pellet
CFQAr	CFQ	Argon	Conical pellet
CFQA	CFQ	Air	Conical pellet

tometer equipped with a graphite monochromator on the diffracted beam.

The spectra of BMAr and BMA samples were recorded on the powders sampled at selected milling times.

In order to perform the XRD and Mössbauer spectra on the samples obtained using the SHS techniques, they were comminuted in a planetary ball mill (Fritsch Pulverisette 5) using agate vials and balls. After milling, little particles of iron ($34 \pm 2\%$ wt and $32 \pm 2\%$ wt for argon and air experiments, respectively) were separated, using a 80 mesh sieve, from the remaining finer powders which were used to carry out XRD and Mössbauer spectra.

In the case of CFQ samples, XRD spectra were performed on a slice (about 1–2 mm thick) of it, which includes the region where the combustion front was arrested, separated from the rest of the sample. Even though the sampling procedure followed does not change, it is very difficult to isolate exactly the same portion of the conical sample to be investigated.

The Mössbauer absorption spectra were obtained in a standard transmission geometry, using a source of ^{57}Co in rhodium (37 MBq). A calibration was performed using a 25 μm thick natural α-Fe foil; the isomer shift values are referred to α-Fe.

The measurements were carried out at room temperature on powder samples contained in a Plexiglas holder. The iron surface density of the absorber for the samples SHSAr and SHSA is 20 and 15 mg/cm^2, respectively; for the BM samples the density is about 15 mg/cm^2.

The absorption spectra of the samples were analysed by fitting the data by curves of Lorentzian shape. The relative spectral contribution of the Fe atoms belonging to each phase has been used to obtain an approximated quantitative evaluation of the composition of the samples [23]. The relative quantity of each phase is expressed as per cent content of Fe atoms.

Optical metallography (OM), SEM and wavelength dispersive spectroscopy (WDS) microanalysis, were also used to characterize SHS and CFQ samples. OM observations were carried out using a Leica REICHERT MEF 4 A/M microscope, while SEM and WDS microanalysis were performed on a ARL SEMQ95 instrument.

3. Results

Figure 2 shows the XRD spectra of BMAr samples at selected milling times. After 1 h milling, all the peaks are still due to the starting crystalline phases, i.e. hematite, aluminum and corundum. After 2 h, peaks due to hercynite ($FeAl_2O_4$) and α-Fe begin to appear while the intensity of Fe_2O_3 and Al peaks decreases. Hercynite peaks grow until 3 h milling time, and then they begin to disappear together with Fe_2O_3 and Al, while the intensity of α-Fe peaks keeps increasing. After 4 h milling Al peaks are no more detectable, those due to hercynite disappear after 6 h milling while Fe_2O_3 peaks are detectable until 8–10 h milling. Milling also induces a broadening of all peaks, due to particle size refinement.

The XRD spectra of BMA samples at selected milling times are shown in Figure 3. After 1 h milling the pattern is very similar to the one of BMAr but after 2 h the two patterns begin to differentiate. In particular the peaks due to hercynite are much more evident in BMA sample from 2 h milling onward and they are still present at the end of the milling together with α-Fe and Al_2O_3 peaks while Fe_2O_3 and Al peaks are no more detectable. α-Fe peaks after reaching a maximum at about 6–8 h milling begin to decrease their intensity. As in BMAr samples, peaks show a broadening with milling time.

Figure 4 shows the XRD spectra of the powders obtained after comminuting SHSAr and SHSA samples and separating the iron particles as described in the experimental section. The two spectra, which are very similar, indicate the presence of corundum, hercynite and traces of iron. All peaks are significantly sharper than those present in the spectra of ball milled samples.

In Fig. 5 the XRD patterns of CFQAr and CFQA samples are reported. In both spectra the same crystalline phases can be identified, i.e. hematite, alu-

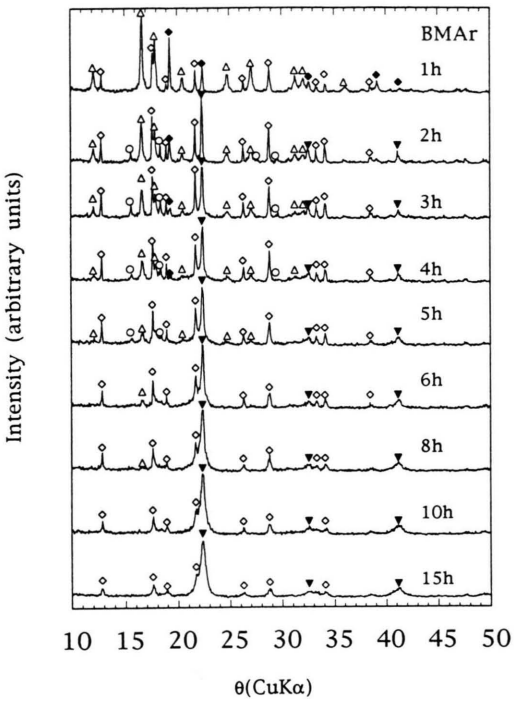

Fig. 2. XRD spectra at selected milling times for BMAr samples: (△) Fe_2O_3, (◆) Al, (◇) Al_2O_3, (○) $FeAl_2O_4$, (▼) Fe.

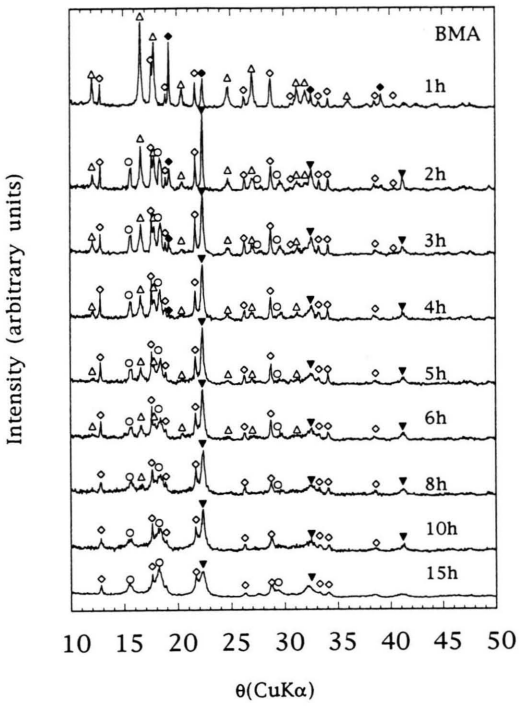

Fig. 3. XRD spectra at selected milling times for BMA samples: (△) Fe_2O_3, (◆) Al, (◇) Al_2O_3, (○) $FeAl_2O_4$, (▼) Fe.

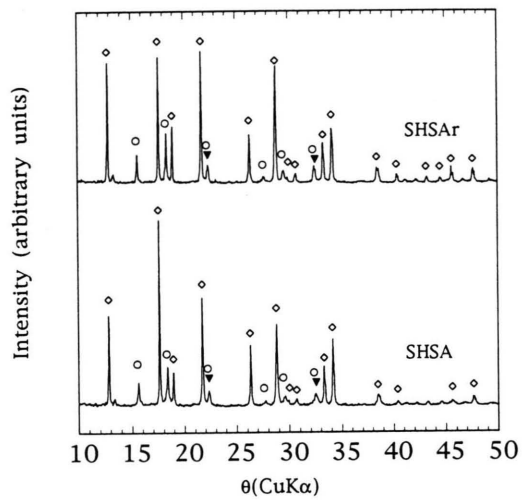

Fig. 4. XRD spectra of the SHSAr and SHSA samples: (◇) Al_2O_3, (○) $FeAl_2O_4$, (▼) Fe.

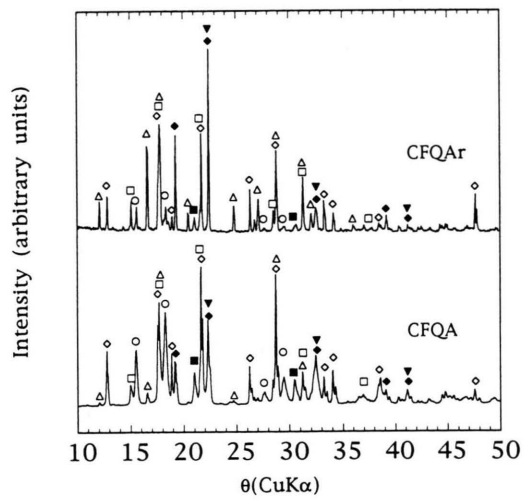

Fig. 5. XRD spectra of the CFQAr and CFQA samples: (△) Fe_2O_3, (□) Fe_3O_4, (■) FeO, (◆) Al, (◇) Al_2O_3, (○) $FeAl_2O_4$, (▼) Fe.

minum, corundum, magnetite, hercynite, wuestite and iron, even if a difference in the relative intensity of the peaks can be observed, partially due to the difficulty in isolating the same quenched region, as discussed in the previous section.

In Fig. 6 the Mössbauer spectra of the samples milled in Ar at selected times are reported, while Fig. 7 shows the spectra of the samples milled in air at the same times. These data have been fitted by Lorentzian curves, plotted as continuous lines in the figures. The resulting evolution of the absorption area of each phase during the milling is given in Figs. 8 a and 8 b for the BMAr and BMA samples, respectively. The area ascribed to Fe_2O_3 can include a contribution of Fe_3O_4, which is not discernible in the spectra [24].

Table 2 reports the results of the least squares fits of the spectra of the final samples (15 h of milling); the values of isomer shift (δ) relative to α-Fe, quadrupole splitting (Δ), internal magnetic field (B), half width at half maximum of the peaks ($\Gamma_1/2$ and $\Gamma_2/2$) and absorption of each phase (Area) are given. The phases have been identified by means of the values of the Mössbauer parameters.

In the BMAr sample after 2 h of milling, the reduction of trivalent iron to metallic (α-Fe, 28%) and divalent iron (hercynite, 9%) is observed [24–26]; another component of reduced iron (6%) is also present. This last component, which corresponds to a single-line with isomer shift − 0.1 mm/s, is ascribed to clusters of iron atoms with size of a few nanometers [27, 28].

The starting hematite disappears at 10 h of milling, while the content of hercynite reaches a maximum at 6 h (21% of the absorption) and then decreases. The α-Fe component increases continuously up to 82% in the final sample, while the content of Fe clusters reaches a maximum of 10% at 4 h.

Table 2. Mössbauer parameters as obtained by fitting the spectra of the ball milled samples. Table shows the values of isomer shift (δ), quadrupole splitting (Δ), magnetic field (B), half width at half maximum of the peaks ($\Gamma_1/2$ and $\Gamma_2/2$) and absorption of each phase (Area).

Sample	Phase	δ mm/s	Δ mm/s	B T	$\Gamma_1/2$ mm/s	$\Gamma_2/2$ mm/s	Area %
BMAr/15 h	α-Fe	0.00		33.2	0.22		82
	$FeAl_2O_4$	1.07	1.77		0.45	0.55	14
	Fe clusters	−0.12			0.14		4
BMA/15 h	α-Fe	0.02		33.2	0.18		21
	$FeAl_2O_4$	1.04	1.57		0.46	0.55	68
	Fe clusters	−0.09			0.21		11

Table 3. Mössbauer parameters as obtained by fitting the spectra of the samples prepared by SHS (fine powder). Table shows the values of isomer shift (δ), quadrupole splitting (Δ), magnetic field (B), half width at half maximum of the peaks ($\Gamma_1/2$ and $\Gamma_2/2$) and absorption of each phase (Area). (f.p. stands for fixed parameters).

Sample	Phase	δ mm/s	Δ mm/s	B T	$\Gamma_1/2$ mm/s	$\Gamma_2/2$ mm/s	Area %
SHSAr	α-Fe	0.00		33.3	0.13		24
	$FeAl_2O_4$	0.95	1.66		0.41	0.43	76
SHSA	α-Fe	0.00		33.3	0.15		17
	Fe_3O_4 f.p.						7
	$FeAl_2O_4$	0.93	1.62		0.44	0.56	76

In the BMA sample after 2 h of milling, the same four phases are present as in the sample milled in Ar, but the content of hercynite is double (19%). The content of hematite is zero at 15 h, while hercynite increases up to 68% after 15 h. The content of α-Fe is maximum at 6 h (31%); then the metal is partially oxidated and decreases to 21% after 15 h. The oxidation in atmosphere of air increases with further milling.

The Mössbauer spectra of the SHS samples were carried out on fine powders obtained by separating the large particles of iron in the final product, as described in the experimental section. Figures 9 a and 9 b show the spectra of the cylindrical pellets prepared in Ar and air, respectively. Table 3 reports the parameters obtained by fitting these data.

The SHSAr sample contains iron atoms in form of α-Fe and hercynite, while the SHSA contains also a small quantity of magnetite. The content of metal iron in the pellet has been evaluated by considering the relative spectral area of the α-Fe in the powder and the relative weights of powders and large particles; this content was found to be (91 ± 3) and (85 ± 3) per cent Fe atoms in the SHSAr and SHSA samples, respectively. This degree of reduction of the iron is very similar to that observed in the BMAr sample at 15 h (86% by considering α-Fe and iron clusters).

The contribution of hercynite in the spectra is given by a quadrupole doublet [25, 26]; this doublet was found to be symmetric in SHSAr pellets and asymmetric in SHSA pellets and in final milled samples. Therefore the spectra have been fitted with an asymmetric Lorentzian doublet [21]; this doublet approximates a distribution of quadrupole doublets, which characterizes the spectrum of hercynite [26], but can be used in the fit of polyphasic spectra. The stoichiometric her-

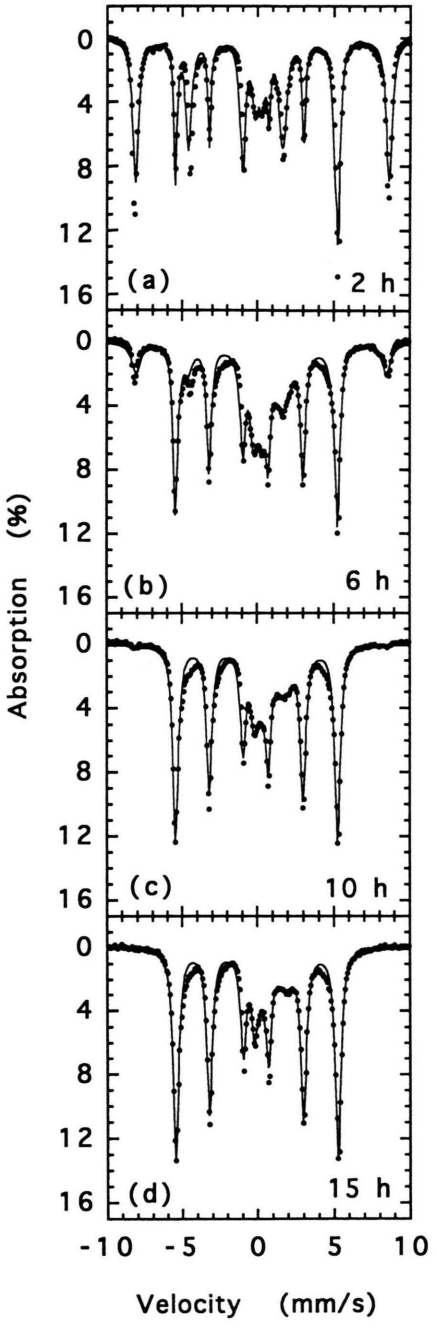

Fig. 6. Mössbauer absorption spectra at selected milling times for the samples prepared in Ar. Experimental data are reported as dots; the solid line shows the fit.

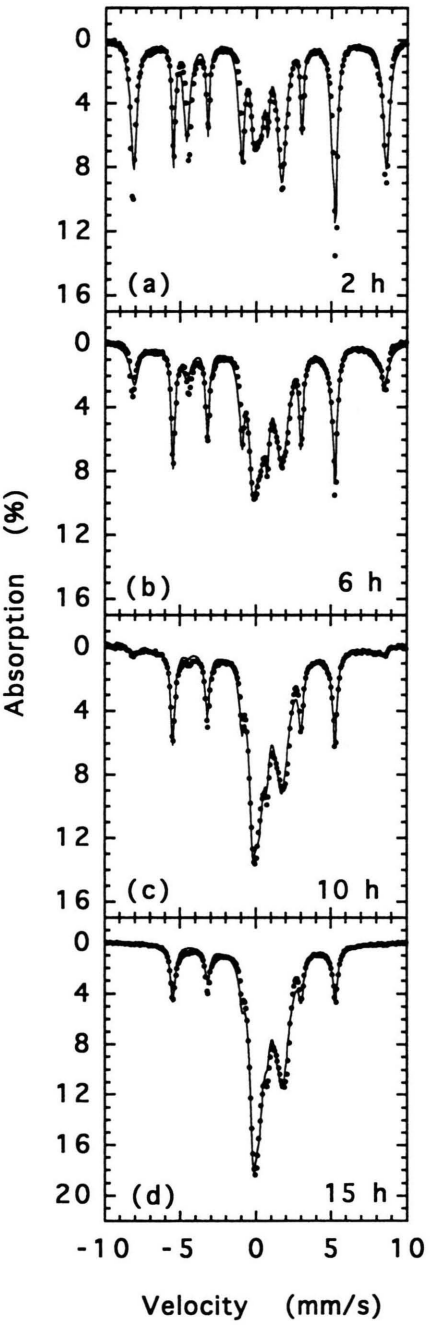

Fig. 7. Mössbauer absorption spectra at selected milling times for the samples prepared in air. Experimental data are reported as dots; the solid line shows the fit.

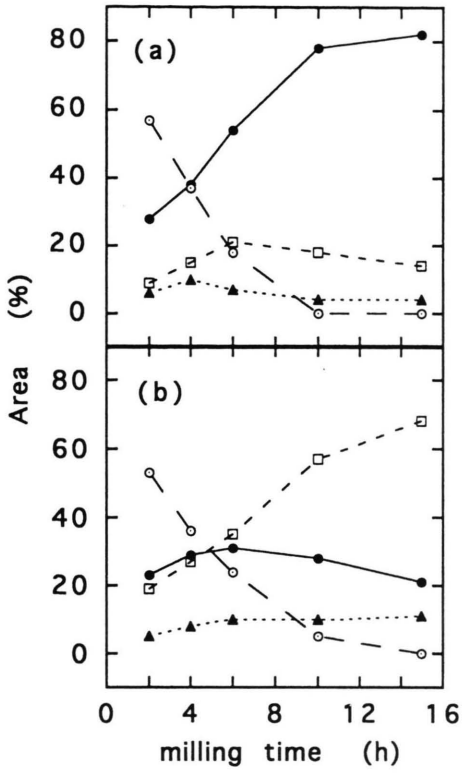

Fig. 8. Phase analysis from Mössbauer spectra, as per cent of the total spectral area, at different milling times in Ar (a) and air (b). The used markers are: open circles for hematite, full circles for α-Fe, squares for hercynite and triangles for Fe clusters.

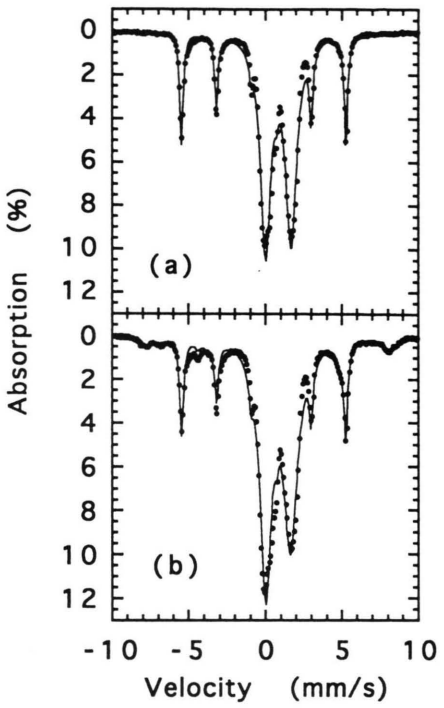

Fig. 9. Mössbauer absorption spectra of the samples prepared by SHS in Ar (a) and air (b). Experimental data are reported as dots; the solid line shows the fit.

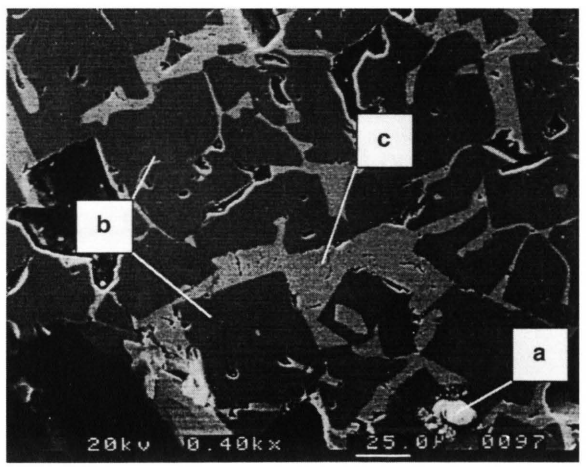

Fig. 10. Back-scattered SEM view of the microstructure of an SHSA sample: iron (a), corundum (b), and hercynite (c).

cynite ($FeAl_2O_4$) gives a symmetric doublet [25, 26]; the asymmetry of the peaks indicates a partial substitution of Al with Fe atoms, according to the formula $Fe_{1+x}Al_{2-x}O_4$, with $x < 0.5$ [29]. In our samples the stoichiometric hercynite forms only in the SHSAr pellet.

A SEM back-scattered micrograph of an SHSA sample, for which the maximum temperature measured during combustion evolution equals 1920 K, is shown in Figure 10. Iron (a), alumina (b) and hercynite (c) are identified by WDS. The microstructure of SHSAr samples does not change with respect to the one shown in Figure 10.

Two SEM back-scattered images of a CFQA sample, showing the region where the combustion front is arrested, are reported in Figure 11. Four zones with different structure and composition may be distinguished and are schematically indicated in the sketch corresponding to the conical samples. Region 1, which represents the unreacted powders, borders region 2 constituted by a light phase of iron oxides (p), where aluminum (m) and alumina (n) particles, surrounded by different iron-aluminates (q), are dispersed. The iron-aluminates may be considered as the result of

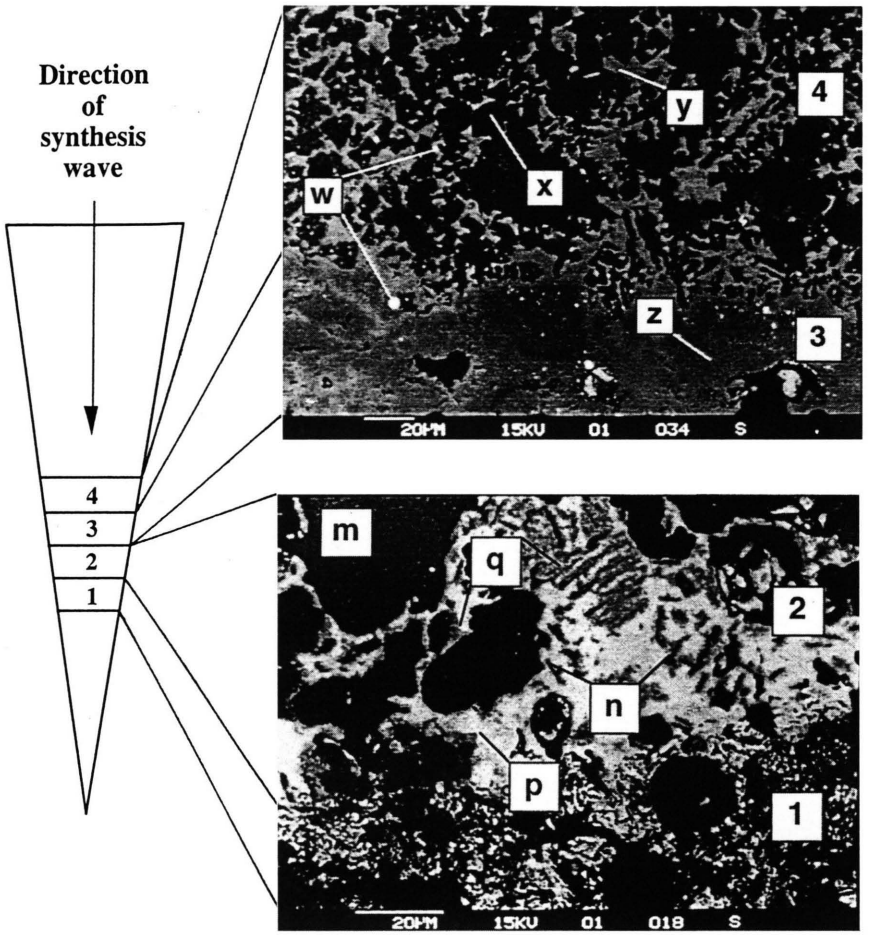

Fig. 11. SEM back-scattered images of CFQA sample and schematic representation of the dynamics of structure and products formation: (m) Al, (n) Al_2O_3, (p) Fe_3O_4, FeO, (q) $FeAl_\alpha O_\beta$, (w) Fe, (z) $FeAl_\gamma O_\delta$ ($\gamma > 2$), (x) Al_2O_3, (y) $FeAl_2O_4$.

the first interaction between the species involved in the aluminothermic reaction. This interaction increases, giving rise to non stoichiometric (atomic ratio Al/Fe > 2) iron-aluminates (z), which mainly constitute region 3. In the same region grains of iron and hercynite start to appear. However, these species are present in larger amounts in the heterogeneous region 4. Alumina is found as corundum (x), whose grains grow up to about 10 μm as the distance from zone 3 increases, being hercynite (y) distributed around these grains. Iron spots (w) appear to be dispersed in region 4. No remarkable differences are observed working under Argon atmosphere. It is worth noting that final products revealed in region 4 correspond to the ones obtained by reacting the same starting mixture without quenching conditions.

3. Discussion

The mechanism of structure and product formation of the aluminothermic reduction of hematite under SHS conditions in air atmosphere and in the presence of 25% of alumina has been recently examined by Orru' et al. [8–9] using the CFQ technique. By taking advantage of the results obtained by Korchagin and Podergin [7], the first steps of the aluminothermic reduction can be described through the following mechanism:

$$3\,Fe_2O_3 \rightarrow 2\,Fe_3O_4 + 1/2\,O_2\,, \tag{1}$$

$$Fe_3O_4 \rightarrow 3\,FeO + 1/2\,O_2\,, \tag{2}$$

$$FeO + Al_2O_3 \rightarrow FeAl_2O_4\,, \tag{3}$$

$$Fe_3O_4 + 2\,Al \rightarrow FeAl_2O_4 + 2\,Fe\,, \quad (4)$$

$$2\,FeO + Al \rightarrow 3/2\,Fe + 1/2\,FeAl_2O_4\,. \quad (5)$$

Note that the reactions

$$Fe_3O_4 + 2/3\,Al \rightarrow 3\,FeO + 1/3\,Al_2O_3\,, \quad (6)$$

$$1/2\,FeAl_2O_4 + 1/3\,Al \rightarrow 1/2\,Fe + 2/3\,Al_2O_3\,, \quad (7)$$

proposed in [7], were not considered as possible steps of the SHS aluminothermic reduction. This is because the reaction was supposed to proceed giving rise to a melt corresponding to the metastable phase of iron-aluminates, shown in region (z) of Fig. 11, from which corundum and hercynite appear to be formed through a crystallization process. Note that both melt formation and subsequent crystallization phenomena are typical of SHS processes [30]. As expected, the final reaction products above are those encountered under SHS experiments, i.e. without quenching conditions.

On the basis of the results obtained in this work, the same mechanism of product and structure formation in SHS conditions summarized above is valid also under argon atmosphere. The only difference is related to the fact that stoichiometric hercynite is found under argon atmosphere, as clearly revealed by Mössbauer spectroscopy. Thus, it may be concluded that SHS is weakly affected by the reaction atmosphere. On the contrary, the percentage of hercynite strongly increases when BM is performed under air where, in addition, the produced iron tends to progressively reoxidize with increasing milling time. The different behaviour is certainly due to the intrinsic difference of reaction time scales typical of the two techniques. In fact, SHS processes are extremely fast so that there is virtually no interaction with the reaction atmosphere, while the reaction evolution is much slower in BM processes, so that reactants and products can also react with the oxygen present in the atmosphere.

It should be noted that, while both XRD analysis and Mössbauer spectroscopy revealed the presence of hercynite in final BMA samples, in the XRD spectrum of BMAr15 sample no traces of hercynite were detected, even if the amount revealed by Mössbauer is about 15 weight %. This amount is larger than the detection limit of X-ray diffraction, but because of the peak broadening due to particle size refinement, it is likely that peaks become undetectable. In the SHS samples the same amount of hercynite gives rise to sharp peaks that are cleary detectable in the XRD spectra, carried out on a portion of the sample reduced to powder after separating the large iron particles.

It should be also noted that Basset et al. [28] obtained the complete reduction of hematite with aluminum by BM both under air and nitrogen. The different result can be ascribed to the excess of corundum present in the samples investigated in the present work and to the different conditions of milling.

In the BM process, hercynite is the only intermediate compound observed, while magnetite and wuestite are also revealed through the CFQ technique as intermediate products of the SHS reaction. However, the formation of lower iron oxides may not be excluded also in the BM techique, where the reaction evolves continuously so that FeO and Fe_3O_4, when formed, are likely to quickly react with the Al_2O_3 that is present in excess.

On the basis of these observations, the possible reaction path for BM, at least under argon atmosphere, may be the one indicated by reactions (1) to (7). Reactions (6) and (7) are here included because they allows us to justify not only the formation of alumina but also the behavior of hercynite content as a function of milling time shown in Figure 8 a. Thus, we conclude that a similar reaction path in SHS and BM reaction under argon atmosphere may be postulated, even if the two preparation procedure are quite different. In particular, the SHS reaction involves the formation of a melt from which the products crystallize, while BM proceeds through solid state reactions and no melting takes place.

Finally, for the case of the aluminothermic reduction of ferric oxide by BM under air atmosphere, the definition of the reaction path clearly calls for the introduction of oxygen as reactant in the kinetic scheme proposed above.

Acknowledgements

The financial support of Regione Autonoma della Sardegna (Italy), MURST and CNR is gratefully acknowledged. We also acknowledge Prof. C. Muntoni for helpful discussions.

[1] L. L. Wang, Z. A. Munir, and Y. M. Maximov, J. Mat. Sci. **28,** 3693 (1993).
[2] A. G. Merzhanov, In Z. A. Munir and J. B. Holt (Eds.), Proc. on Int. Symp. on Combustion and Plasma Synthesis of High Temperature Materials, VCH Publishers, New York **1990,** p. 1.
[3] O. Odawara, J. Amer. Ceram. Soc. **73,** 629 (1990).
[4] S. Yin, M. Liu, C. Yao, and Z. Guo, Int. J. of SHS **2,** 69 (1993).
[5] S. Chandran, S. K. Jagarlamudi, and J. A. Puszynski, In P. Vincenzini (Ed.), Proc. of the 8th CIMTEC-World Ceramics Congress and Forum on New Materials – Ceramics: Charting the Future Vol. **3C,** Techna Publ., Faenza **1995,** p. 2005.
[6] R. Orru', B. Simoncini, P. F. Virdis, and G. Cao, Int. J. of SHS **4,** 137 (1995).
[7] M. A. Korchagin and V. A. Podergin, Comb. Explos. Shock Waves (Engl. transl.) **15,** 325 (1979).
[8] R. Orru', B. Simoncini, P. F. Virdis, and G. Cao, Metall. Sci. Tech. **14(2),** 69 (1996).
[9] R. Orru', B. Simoncini, P. F. Virdis, and G. Cao, Chem. Engng. Comm., in press (1997).
[10] Z. A. Munir and U. Anselmi-Tamburini, Mater. Sci. Rep. **3,** 277 (1989).
[11] A. Varma and J. P. Lebrat, Chem. Engng. Sci. **47,** 2179 (1992).
[12] G. Cao and M. Morbidelli, Chim. Ind. Milan **75,** 3 (1993).
[13] A. G. Merzhanov, Int. J. SHS **2,** 113 (1993).
[14] J. B. Holt, J. Wong, E. Larson, P. Waide, B. Rupp, and R. Frahm, In Kaieda and Holt **1990,** p. 107.
[15] A. S. Mukasyan and I. P. Borovinskaya, Int. J. SHS **1,** 55 (1992).
[16] C. C. Koch, In Material Science and Technology: A Comprehensive Treatment, edited by R. W. Cahn, P. Haasen, and E. J. Kramer (VCH Verlagsgesellschaft, Weinheim 1991) Vol. **5,** Chapt. 5.
[17] F. H. Froes and J. J. de Barbadillo, Structural Applications of Mechanical Alloying (ASM International, Metals Park, Ohio 1993).
[18] P. Matteazzi and G. L. Le Caer, Hyperfine Interact. **68,** 177 (1991).
[19] D. Basset, P. Matteazzi, and F. Miani, Mater. Sci. Eng. **A168,** 149 (1993).
[20] L. Takacs, Nanostr. Mater. **2,** 241 (1993).
[21] G. Concas, F. Congiu, A. Corrias, C. Muntoni, G. Paschina, and D. Zedda, Z. Naturforsch. **51a,** 915 (1996).
[22] A. Corrias, G. Ennas, A. Musinu, G. Paschina, and D. Zedda, J. Mater. Res. submitted for publication (1997).
[23] C. Janot, L'Effect Moessbauer et ses Applications, Masson et Cie, Paris **1972,** p. 201.
[24] J. Danon, In Chemical Applications of Moessbauer Spectroscopy, eds. V. I. Goldanskii and R. H. Herber, Academic Press, New York **1968,** p. 159.
[25] J. L. Dormann, M. Seqqat, D. Fiorani, M. Nogues, J. L. Sobeyroux, S. C. Bhargava, and P. Renaudin, Hyperfine Interact. **54,** 503 (1990).
[26] P. Matteazzi and G. L. Le Caer, J. Amer. Ceram. Soc. **75,** 2749 (1992).
[27] C. Donnet, G. Marest, N. Moncoffre, and J. Tousset, Nucl. Instr. and Meth. **B59/60,** 1177 (1991).
[28] D. Basset, P. Matteazzi, F. Miani, and G. L. Le Caer, Hyperfine Interact. **94,** 2235 (1994).
[29] G. Dehe, B. Seidel, K. Melzer, and C. Michalk, Phys. Stat. Solidi (a) **31,** 439 (1975).
[30] P. V. Zhirkov and A. Yu. Dovzhenko, Int. J. of SHS, **3,** 167 (1994).